Following an isosymmetric phase transition by changes in bond lengths and anisotropic displacement parameters: the case of meta -carboxyphenylammonium phosphite

El-Eulmi Bendeif, Claude Lecomte, Slimane Dahaoui

Acta Crystallographica Section B
Structural Science
ISSN 0108-7681

Following an isosymmetric phase transition by changes in bond lengths and anisotropic displacement parameters: the case of *meta*-carboxyphenylammonium phosphite

El-Eulmi Bendeif,[a,b] Claude Lecomte[a] and Slimane Dahaoui[a]*

[a]Laboratoire de Cristallographie et Modélization des Matériaux Minéraux et Biologiques LCM3B CNRS UMR 7036, Institut Jean Barriol Nancy Université, Faculté des Sciences, BP 239, 54506 Vandoeuvre-lès-Nancy CEDEX, France, and [b]Synchrotron Soleil, L'Orme des Merisiers, Saint-Aubin, BP 48, 91192 Gif-sur-Yvette CEDEX, France

Correspondence e-mail: slimane.dahaoui@lcm3b.uhp-nancy.fr

Received 25 June 2008
Accepted 11 December 2008

Crystal structure studies in the 100–345 K temperature range were performed to relate the molecular structure changes of *meta*-carboxyphenylammonium phosphite (*m*-CPAMP) to its first-order phase transition at T_c = 246 (2) K. Thermal displacement parameters and most bond distances show an abrupt jump at the transition. Such a structural change is related to collective effects leading to competition between intra- and intermolecular interactions.

1. Introduction

Variable-temperature crystal-structure studies of several phosphate compounds that exhibit interesting physical properties have been performed in our laboratory (Boukhris *et al.*, 1994, 1998; Souhassou *et al.*, 1995; Delarue *et al.*, 1998, 1999). The system $R(H_2PO_4)$ was the most intensively investigated system. Well known examples are the potassium dihydrogen phosphate KH_2PO_4 (KDP), which undergoes a paraelectric to ferroelectric phase transition at $\sim$122.5 K (Baur, 1973; Kobayashi *et al.*, 1970), and ammonium dihydrogen phosphate $NH_4H_2PO_4$ (ADP), which exhibits a paraelectric to-antiferroelectric phase transition at 148 K (Keeling & Pepinsky, 1955; Boukhris *et al.*, 1994). Since glycinium phosphite (GPI) and betainium phosphite (BPI) were introduced as interesting ferroelectric materials (Albers *et al.*, 1988; Baran *et al.*, 1997), many phosphate and phosphite salts have received considerable attention. However, detailed structural studies *versus* temperature on phosphite salts are very scarce.

Recently, we have reported on an original isosymmetric single-crystal phase transition at 246 (2) K in a new phosphite salt (*m*-carboxyphenylammonium monohydrogenphosphite, *m*-CPAMP, $C_7H_8NO_2^+$, HPO_3H^-) (Bendeif *et al.*, 2005).[1] On the basis of the temperature evolution of the unit-cell parameters, this isosymmetric phase transition was shown to be reversible and first-order with a hysteresis of 3.6 K (see Fig. 4 **(AUTHOR - fig. 4 of this paper or 2005)**, Bendeif *et al.*, 2005). Although the phase transition induces a significant reorganization of the molecular packing (see Figs. 8 and 9 **(AUTHOR - figs 8 and 9 of this paper or 2005?)**; Bendeif *et al.*, 2005) without any symmetry breaking, the phase transition mechanism and its origin have not been clarified. At this point the need was evident to perform temperature-dependent experiments to follow the changes induced in the molecular and intermolecular interactions.

The present study of *m*-CPAMP covers the temperature range 100–345 K and discusses unexpected evolutions of the

[1] In our first paper (Bendeif *et al.*, 2005), we reported the possible occurrence of weak satellite reflections which we wanted to confirm by synchrotron measurements. However, despite many trials on several crystals at HASYLAB we were unable to see any satellite reflections.

intra- and intermolecular distances as well as the mean-square displacement parameters *versus* temperature (Fig. 1).

2. Experimental section

2.1. Crystal growth

Crystals of *m*-CPAMP were obtained by mixing a solution of phosphorous acid (30%) with an aqueous solution of *m*-amino benzoic acid, $NH_2C_6H_4COOH$, in stoichiometric ratios. The resulting aqueous solution was then kept at room temperature. After a few days of slow evaporation, large brown plate-shaped single crystals appeared in the solution.

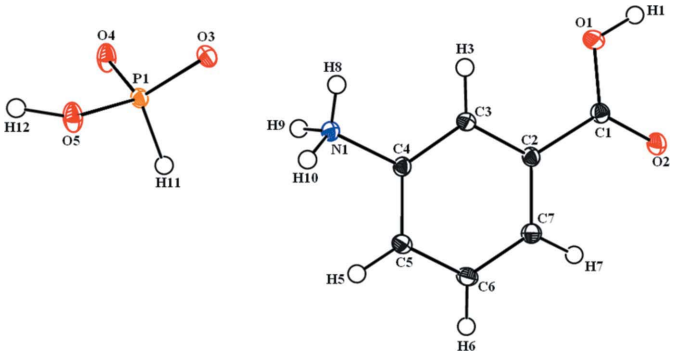

Figure 1
Molecular structure of *m*-CPAMP in the crystal. *ORTEP*III representation (Burnett & Johnson, 1996) with thermal displacement ellipsoids plotted at 50% probability. H atoms are represented by spheres.

2.2. Single-crystal X-ray diffraction

The temperature-controlled X-ray diffraction experiments were performed on a single-crystal Oxford Sapphire 2 four-circle automatic diffractometer equipped with an area detector and an Oxford Cryosystems Cryostream cooler, using Mo Kα radiation (λ = 0.71073 Å). All measurements were carried out on the same crystal specimen (0.4 × 0.4 × 0.2 mm^3) at nine different temperatures before and after the phase transition, respectively, in the following order: 100, 130, 170, 210, 235, 255, 293, 320 and 345 K. For the high-temperature data collection, we used a locally modified gas-stream heating device (Tuinstra & Storm, 1978). The temperature stability was within ±0.2 K during the time of the measurements. After each temperature change the crystal of *m*-CPAMP was allowed to stabilize at the new temperature for 25 min before starting the data collection.

Intensity data were accurately collected using ω step scans with a scan width of 1° per frame repeated at eight different φ positions; the sample-to-detector distance was 45 mm. This procedure yields a completeness of datasets that exceeds 98% to [$(\sin\theta/\lambda)_{max}$ = 0.7 Å^{-1}]. A visual examination of the crystal at the end of the experiments showed that it was not damaged by the cooling and heating procedures.

2.3. Data reduction

X-ray data were integrated using the *CrysAlis Red* program (Oxford Diffraction, 2006). The absorption was small, but the data were nevertheless corrected by means of Gaussian

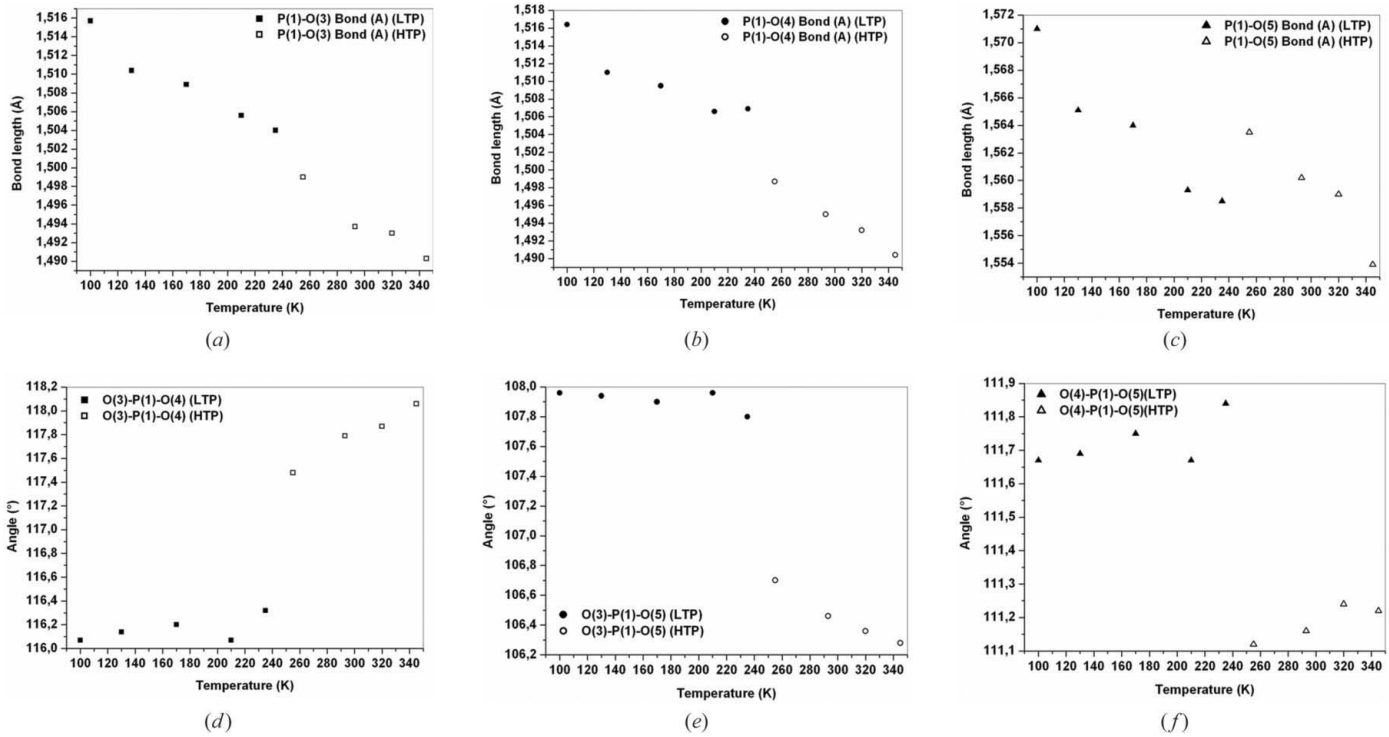

Figure 2
Evolution of $[HPO_3H]^-$ distances (*a*), (*b*) and (*c*), and angles (*d*), (*e*) and (*f*) as a function of temperature. The standard deviation is 2 × 10^{-3} Å and 0.1°.

Table 1
Main crystallographic features, X-ray diffraction data collection parameters and final results for *m*-CPAMP.

The data for the measurements at 100, 170, 210 and 293 K have been deposited with the Cambridge Crystallographic Data Centre (CCDC), 12 Union Road, Cambridge, England. **(AUTHOR - not needed as data deposited with IUCr)**

	130 K	235 K	255 K	320 K	345 K
Crystal data					
Chemical formula	$C_7H_8NO_2^+\cdot H_2PO_3^-$	$C_7H_8NO_2^+\cdot H_2PO_3^-$	$C_7H_8NO_2^+\cdot H_2PO_3^-$	$C_7H_8NO_2^+\cdot H_2PO_3^-$	$C_7H_8NO_2^+\cdot H_2PO_3^-$
M_r	219.13	219.13	219.13	219.13	219.13
Cell setting, space group	Monoclinic, $P12_1/c1$	Monoclinic, $P12_1/c1$	Monoclinic, $P12_1/c1$	Monoclinic, $P12_1/c1$	Monoclinic, $P12_1/c1$
Temperature (K)	130 (2)	235 (2)	255 (2)	320 (2)	345 (2)
a, b, c (Å)	12.1342 (7), 12.3851 (6), 6.3821 (4)	12.2487 (9), 12.3265 (8), 6.4290 (5)	13.0119 (14), 11.5643 (13), 6.6123 (7)	13.0363 (8), 11.5204 (7), 6.6446 (5)	13.0221 (11), 11.5012 (8), 6.6489 (5)
β (°)	100.299 (5)	100.981 (6)	104.433 (9)	104.826 (6)	104.614 (7)
V (Å^3)	943.67 (9)	952.90 (12)	963.57 (18)	964.69 (11)	963.59 (13)
Z	4	4	4	4	4
D_x (Mg m^{-3})	1.542	1.527	1.511	1.509	1.510
Radiation type	Mo $K\alpha$	Mo $K\alpha$	Mo $K\alpha$	Mo $K\alpha$	Mo $K\alpha$
μ (mm^{-1})	0.29	0.28	0.28	0.28	0.28
Crystal form, colour	Plate, brown	Plate, brown	Plate, brown	Plate, brown	Plate, brown
Crystal size (mm)	0.40 × 0.40 × 0.20	0.40 × 0.40 × 0.20	0.40 × 0.40 × 0.20	0.40 × 0.40 × 0.20	0.40 × 0.40 × 0.20
Data collection					
Diffractometer	Xcalibur-Saphire2	Xcalibur-Saphire2	Xcalibur-Saphire2	Xcalibur-Saphire2	Xcalibur-Saphire2
Data collection method	ω	ω	ω	ω	ω
Absorption correction	Integration	Integration	Integration	Integration	Integration
T_{min}	0.908	0.889	0.872	0.901	0.896
T_{max}	0.938	0.940	0.946	0.943	0.946
No. of measured, independent and observed reflections	23 422, 2732, 2424	23 700, 2765, 2311	25 199, 2814, 2432	21 224, 2816, 2243	24 042, 2815, 2224
Criterion for observed reflections	$I > 2\sigma(I)$	$I > 2\sigma(I)$	$I > 2\sigma(I)$	$I > 2\sigma(I)$	$I > 2\sigma(I)$
R_{int}	0.031	0.033	0.056	0.035	0.049
θ_{max} (°)	30.0	30.0	30.0	30.0	30.0
Refinement					
Refinement on	F^2	F^2	F^2	F^2	F^2
$R[F^2 > 2\sigma(F^2)]$, $wR(F^2)$, S	0.034, 0.094, 1.06	0.039, 0.113, 1.10	0.050, 0.143, 1.08	0.047, 0.149, 1.14	0.049, 0.156, 1.12
No. of reflections	2732	2765	2814	2816	2815
No. of parameters	167	167	167	167	167
Weighting scheme	$w = 1/[\sigma^2(F_o^2) + (0.0603P)^2 + 0.2511P]$, where $P = (F_o^2 + 2F_c^2)/3$	$w = 1/[\sigma^2(F_o^2) + (0.0777P)^2]$, where $P = (F_o^2 + 2F_c^2)/3$	$w = 1/[\sigma^2(F_o^2) + (0.0913P)^2 + 0.1968P]$, where $P = (F_o^2 + 2F_c^2)/3$	$w = 1/[\sigma^2(F_o^2) + (0.0944P)^2 + 0.0131P]$, where $P = (F_o^2 + 2F_c^2)/3$	$w = 1/[\sigma^2(F_o^2) + (0.0944P)^2 + 0.0131P]$, where $P = (F_o^2 + 2F_c^2)/3$
$(\Delta/\sigma)_{max}$	0.04	0.029	0.062	0.009	<0.0001
$\Delta\rho_{max}$, $\Delta\rho_{min}$ (e Å^{-3})	0.44, −0.29	0.46, −0.27	0.39, −0.39	0.53, −0.28	0.49, −0.26

Computer programs used: *CrysAlis CCD/RED* (Oxford Diffraction, 2006), *SHELXS*97 (Sheldrick, 2008), *ORTEP*III (Burnett & Johnson, 1996), *WinGX* (Farrugia, 1999).

numerical integration using the *ABSORB* program (DeTitta, 1985). Details on data reduction are given in Table 1.

2.4. Crystal structure refinements

All crystal structures were solved in the $P2_1/c$ space group by direct methods and refined by full-matrix least-squares on F^2 using *SHELXL*97 (Sheldrick, 2008), with no constraints applied. All calculations were carried out using the *WinGX* software package (Farrugia, 1999). Atomic scattering factors were taken from the *International Tables for Crystallography* (1992, Vol. C, Tables 4.2.6.8 and 6.1.1.4). Non-H atoms were refined anisotropically using all reflections with $I > 2\sigma(I)$. All H atoms were located in Fourier difference maps and refined isotropically. Rigid body analysis (Cruickshank, 1956; Schomaker & Trueblood, 1968), including a non-rigid attached rigid group (Dunitz & White, 1973; Trueblood, 1978; Dunitz *et al.*, 1988; Schomaker & Trueblood, 1998), was performed using *THMA*11 (Trueblood, 1990). The full experimental details and refinements results for the structure at five temperatures are summarized in Table 1; information about the structure at the other four temperatures is available with the supplementary material.[2]

[2] Supplementary data for this paper are available from the IUCr electronic archives (Reference: BK5076). Services for accessing these data are described at the back of the journal.

3. Results and discussion

m-CPAMP (see Fig. 5 **(AUTHOR - fig 5 of this paper or 2005?**, Bendeif *et al.*, 2005) undergoes a reversible first-order transition at T_c = 246 (2) K with a hysteresis of 3.6 K (Bendeif *et al.*, 2005). All cell parameters show abrupt changes at 246 (2) K, which are more pronounced for **a** and **b** ($\Delta a/a$ = 6.87% and $\Delta b/b$ = -7.7%) than for **c** ($\Delta c/c$ = 3.8%). The β angle also changes significantly from 100.122 (5) to 104.73 (3)° ($\Delta\beta/\beta$ = 4.4% at T_c). The volume expands by 1.77% at T_c. The metrics and the space group remain the same, $P2_1/c$, $Z = 4$ over the 95–335 K range, and the phase transition is classified as isosymmetric or isostructural (Herbstein, 2006; Brittain, 2006).

The ionic structure can be described as alternating layers of $[HPO_3H]^-$ anions and $[NH_3C_6H_4COOH]^+$ cations perpendicular to the **c** direction. The arrangement is characterized by centrosymmetric $[HPO_3H]_2^{2-}$ dimers and the crystal is stabilized by a three-dimensional network of hydrogen bonds which links anionic dimers and cationic layers; for more detail see Bendeif *et al.* (2005).

3.1. Evolution of bond distances and angles with temperature

3.1.1. The phosphite dimer. Fig. 2 shows the evolution of some characteristic phosphite group distances and angles as a function of temperature. Both the P1═O3 and P1═O4 bond distances show a similar behaviour *versus* temperature: they decrease with temperature with a mean jump of 0.026 (1) Å at the transition temperature T_c = 246 (2) K; the P—O5(H) bond length also decreases with temperature in the LTP but with an anomalous behaviour at T_c [increase by 0.005 (1)] then decrease again in the HTP.

This bond strengthening with temperature is related to the O—P1—O and O—P1—OH angles, which decrease on average by 1.105 (9)°, whereas O3—P1—O4 increases by 1.99 (9)°. This is a consequence of the repulsion between the O3 and O4 atoms, which is larger when the P—O bond shortens.

These changes have dramatic consequences for the $[HPO_3H]_2^{2-}$ dimer conformation (Fig. 3): whereas the P1, O4, O5, P1′, O4′ and O5′ atoms are strictly coplanar in the low-temperature phase (LTP), in the high-temperature phase (HTP) the phosphorus atoms P1 and P1′ are displaced by 0.352 Å from the mean plan defined by the O atoms (O4, O5, O4′ and O5′). The two $[HPO_3H]^-$ entities yielding the $[HPO_3H]_2^{2-}$ dimer approach each other along the **b** direction, consequently, the P1—P1′ distance decreases by 0.086 (2) Å at T_c = 246 (2) K in correlation with the significant shortening of the **b** unit-cell parameter with increasing temperature [from 12.3265 (8) Å at 235 K to 11.5643 (13) Å at 255 K]. This change has interesting consequences for the hydrogen-bond system (see below).

3.1.2. The organic cation. As observed for the $[HPO_3H]^-$ group, increasing the temperature also seems to strengthen the covalent bonds in the organic cation: the average bond distance decreases by 0.012 (2) Å at T_c, whereas the unit-cell volume increases (Fig. 3*a*, supplementary material); the most important change concerns the C2—C3 bond length [0.019 (1) Å; Fig. 4] reinforcing its π character. The C1═O2 and C1—O1H distances which are involved in hydrogen bonds also shorten with temperature by 0.016 (1) and 0.018 (1) Å, respectively (Figs. 3*b* and *c*, supplementary material).

One has to note that these contractions are not a consequence of the absence of a correction of thermal motion since such a correction is within 0.001 Å (LTP) and 0.003 Å (HTP), as shown below by the TLS analysis of the thermal displacement parameters.

3.2. Crystal packing and hydrogen bonds

The crystal packing results from several intermolecular contacts involving both carboxylic and ammonium groups. The strength of these intermolecular contacts changes with temperature, in the range 100–345 K and is correlated with the evolution of the cell parameters: *b* decreases by 7.7%, whereas

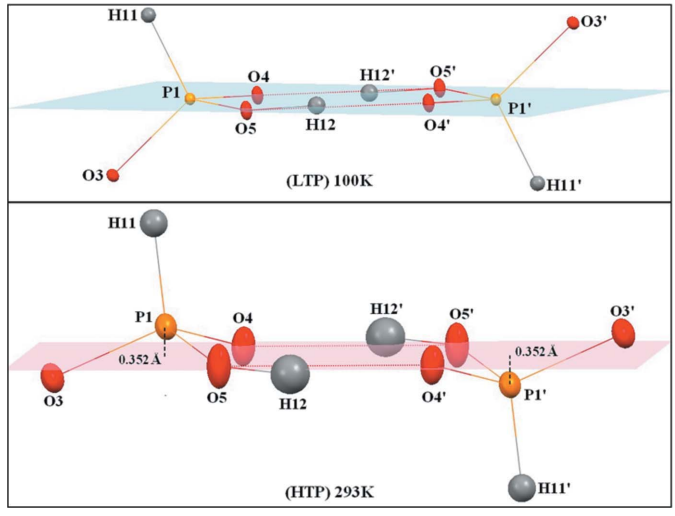

Figure 3
$[HPO_3H]_2^{2-}$ dimer configuration in both LTP and HTP.

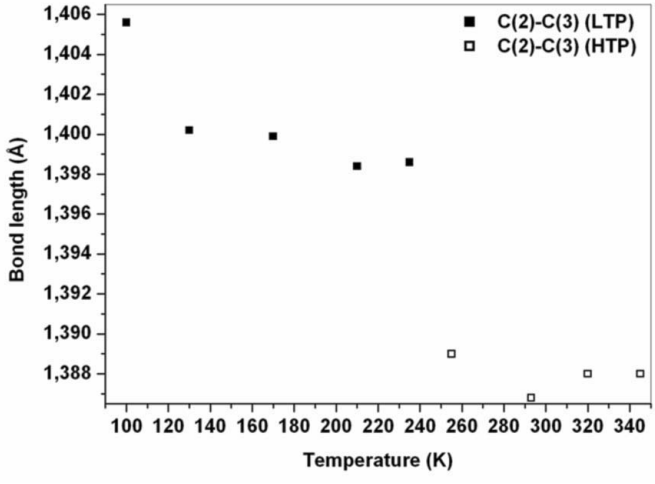

Figure 4
C2—C3 bond-length variation *versus* temperature. The standard deviation is 1×10^{-3} Å.

a and *c* increase by 6.9 and 3.8%, respectively, as discussed previously (Bendeif *et al.*, 2005).

The O(N)—H···O(N) distances (Fig. 5) increase for the O5···O4 and N1···O3 hydrogen bonds, whereas the distances for the N1···O4 and N1···O2 hydrogen bonds decrease with increasing temperature. The O1···O3 distance remains approximately unchanged. As shown in Fig. 4(*a*), the shortest hydrogen bond O5···O4 increases with temperature with an abrupt jump at $T_c = 246$ (2) K; also the strength of the weakest hydrogen bond (N1—H10···O3) approximately parallel to the *c* axis decreases, as shown by the large increase of the N1···O3 distance [from 2.8204 (15) Å at 235 K to 2.8585 (18) Å at 255 K; Fig. 5*b*] and then the signature of the transition is clearly shown around 246 (2) K. In contrast, the N1···O4 and N1···O2 hydrogen bonds decrease by 0.027 (2) Å (0.97%) and 0.023 (2) Å (0.82%), respectively, and therefore strengthen with *T* (Figs. 5*c* and *d*, supplementary material). A more detailed study of the hydrogen-bond angles cannot be performed without data from neutron diffraction experiments.

In summary, when the LTP → HTP transition occurs, the main changes are the following: the P—O bonds strengthen with temperature, as do the bonds of the organic cation. Consequently, the strength of the O5···O4 and N1···O3 hydrogen bonds decreases. These variations clearly indicate a cooperative balance between the covalent character of the anion's and cation's intramolecular bonds and the intermolecular interactions. Such a subtle molecular change (≃ 0.02 Å) has a dramatic consequence for the collective behaviour of the crystal and is evidence of long-range cooperative effects, which are also seen in the analysis of the thermal displacement parameters.

3.3. Thermal motion analysis

3.3.1. Isotropic displacement parameters. If the harmonic mean-square displacements are given by a hyperbolic cotangent function, then each *U* parameter should be proportional to the temperature in the high-temperature limit (Cyvin, 1968; Bürgi *et al.*, 2000). The extrapolation of *U* at $T = 0$ K should be found positive and very small, assigned to the zero-point vibration.

Fig. 6 displays the evolution of the $[HPO_3H]^-$ non-hydrogen isotropic thermal displacement parameters (ITDP). The average value *versus T* for each atom type (non-hydrogen atoms) may be fitted by two linear functions one below T_c and one above. These variations clearly show the existence of the low- and high-temperature phases. As observed for interatomic interactions, the LTP → HTP phase transition is again associated with marked slope changes and systematic abrupt jumps at T_c = 246 (2) K for all thermal displacement parameters. It has to be noted that in the HTP, the O3 straight line interpolates to a negative value (−0.0061 Å^2) at $T = 0$ K (**Fig. 6**), which is physically meaningless in the harmonic approximation. After the transition, in the LTP, (O3) extrapolates to +0.0032 Å^2 at $T = 0$ K and its behaviour is almost equivalent to that of the other phosphite atoms. This negative value is related to the P—O3 and N1···O3 interactions whose strengths are the most affected by the transition. Accurate

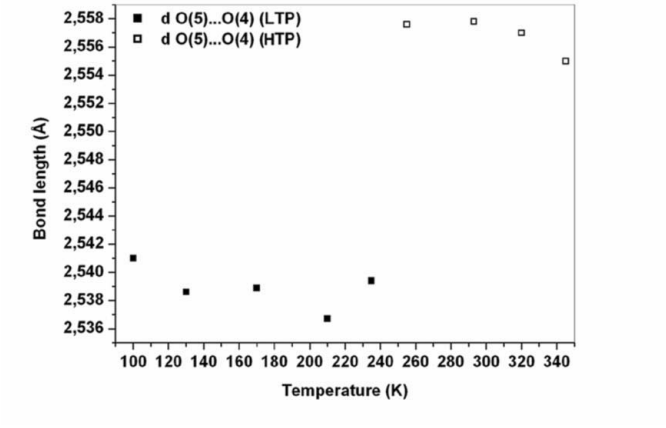

Figure 5
Variation of the O(N)—H···O(N) distances *versus* temperature. (*a*) O5···O4 and (*b*) N1···O3 distances.

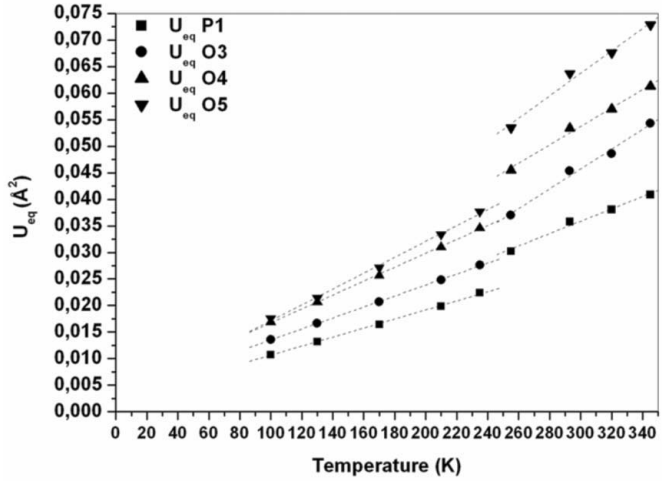

Figure 6
Evolution of the isotropic thermal displacement parameters for the $[HPO_3H]^-$ anion.

analysis of anisotropic displacements parameters (ADP) as a function of temperature gives more insight as shown below.

The variation of the isotropic thermal displacement parameters (ITDP) of the organic cation (Figs. 6*a* and *b*, supplementary material), is similar to that of the phosphite anion. All parameters increase linearly with temperature and the phase transition is characterized by slope changes and abrupt jumps around the transition.

3.3.2. Behaviour of the anisotropic displacement parameters with temperature. In order to analyze the temperature evolution of anisotropic displacements parameters (ADP) of (*m*-CPAMP) below and above the temperature transition (LTP) and (HTP), respectively, each principal anisotropic displacement parameter U^{ii} was plotted against temperature for all non-H atoms. Below T_c, in the LTP, all U^{11}, U^{22} and U^{33} values vary linearly with temperature (Fig. 7*a–m*, supplementary material). Linear extrapolations of U^{11}, U^{22} and U^{33} at $T = 0$ K give an estimate of the static disorder (1.9–5 $\times$ 10^{-3} Å^2, 0.3–4.4 $\times$ 10^{-3} Å^2 and 2–4 $\times$ 10^{-3} Å^2, respectively. The (LTP) $\rightarrow$ (HTP) phase transition is also associated with large jumps of all U^{ii} parameters at T_c. All U^{ii} (O3) extrapolate to negative values in the HTP, contrary to the LTP as expected (Fig. 7).

Furthermore, for all non-H atoms, U^{33} (HTP) extrapolates to negative values (see Figs. 7, supplementary material) contrary to LTP. This anomaly is also a clear indicator of the need of a structural reorganization even though the HTP is ordered.

Then the harmonic model of the thermal displacement parameters may not be valid when extrapolated to 0 K. One can suppose that this negative extrapolated value is the evidence for some anharmonicity (see, for example, Bürgi *et al.*, 2000). A new refinement including higher-order Gram–Charlier terms for all non-H atoms did not improve the refinement statistics and led to insignificant anharmonic terms even just before (235 K) and after (255 K) T_c. In fact, when the phase transition occurs all atoms undergo larger motions in the HTP than in the LTP. This increase requires a structural rearrangement.

3.3.3. Rigid-body model of anisotropic displacement parameters. As discussed above, the investigations of the slope variations for all non-H atoms suggest that the molecule is not entirely rigid and therefore internal vibration modes contribute significantly to the observed mean-square displacements (Rosenfield *et al.*, 1978). In order to obtain better insight into the thermal behaviour of *m*-CPAMP, the least-squares analysis of the rigid-body motion of the molecule in the LTP and HTP was carried out according to the model of Schomaker & Trueblood (1968). The program *THM11* based on the method proposed by Schomaker & Trueblood (1968) and Dunitz & White (1973) performs a TLS analysis, where T accounts for translation, L for libration and S for correlation between molecular translation and libration in the case of a non-centrosymmetric molecule. The inertial axes I_1, I_2 and I_3 of the *m*-CPA cation with respect to the crystallographic axes system are shown in Fig. 8(*a*). The I_1 inertial axis lies nearly along the C1—C2 bond in the phenyl ring plane, the I_2 axis is orthogonal to I_1 and lies in the phenyl ring plane, and the I_3

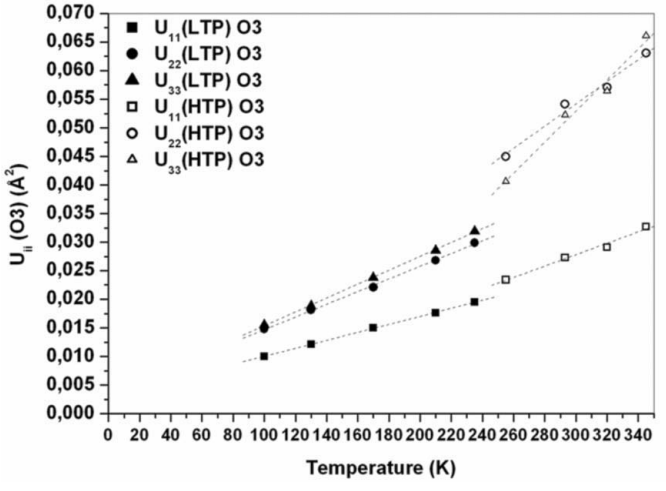

Figure 7
Temperature change of the principal anisotropic displacement parameter of O3.

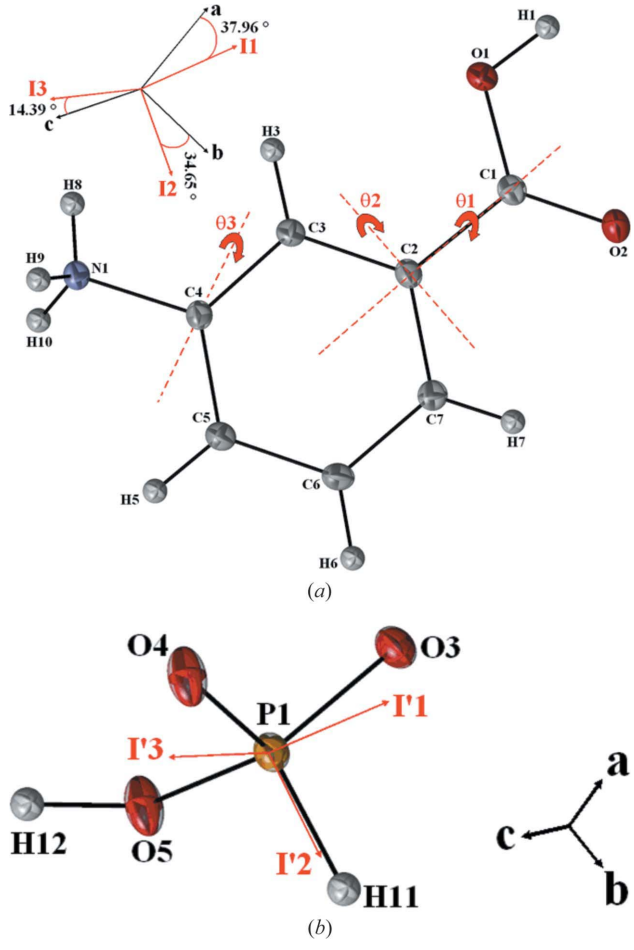

Figure 8
Internal vibration modes and orientation of the inertial and crystallographic axes with respect to (*a*) the *m*-CPA cation and (*b*) the $[HPO_3H]^-$ anion.

Table 2
The values of the rigid-body T (Å^2), L ($^{\circ 2}$) and S (rad Å) of the organic cation in the 100-345 K temperature range in the inertial coordinate system.

θ1, θ2 and **Γ1** and **Γ2** are respectively the internal motions and the mean-square amplitudes of the overall motions of the carboxylic group about the (C5—C2) torsion axis.

T(K)	100	130	170	210	235	255	293	320	345
$T11$	0.0101 (8)	0.0119 (9)	0.0144 (9)	0.017 (1)	0.019 (1)	0.026 (1)	0.031 (2)	0.033 (1)	0.0353 (1)
$T12$	0.0004 (2)	0.0007 (2)	0.0007 (2)	0.0011 (2)	0.0010 (2)	0.0025 (3)	0.0029 (4)	0.0022 (3)	0.0021 (2)
$T13$	−0.0006 (3)	−0.0007 (3)	−0.0011 (4)	−0.0015 (4)	−0.0021 (4)	−0.0019 (4)	−0.0022 (6)	−0.0028 (5)	0.0028 (8)
$T22$	0.0113 (2)	0.0138 (1)	0.0168 (1)	0.0198 (1)	0.0220 (1)	0.0277 (1)	0.0315 (2)	0.0328 (2)	0.0347 (2)
$T23$	0.0005 (2)	0.0006 (7)	0.00097 (8)	0.0014 (1)	0.0013 (1)	0.0005 (1)	0.0008 (2)	0.0004 (1)	−0.0005 (3)
$T33$	0.0118 (1)	0.0139 (1)	0.0173 (1)	0.0210 (2)	0.0237 (2)	0.0278 (2)	0.0318 (3)	0.0353 (2)	0.0383 (7)
$L11$	3.84 (1.72)	5.26 (1.92)	6.78 (2.18)	9.51 (2.50)	10.24 (2.59)	9.11 (2.54)	11.42 (3.63)	11.26 (3.043)	13.10 (2.41)
$L12$	0.86 (0.36)	1.12 (0.40)	1.29 (0.45)	2.11 (0.65)	2.02 (0.53)	2.80 (0.49)	3.73 (0.69)	3.95 (0.58)	4.04 (0.40)
$L13$	0.41 (0.63)	0.76 (0.70)	1.14 (0.80)	1.51 (0.84)	1.91 (0.95)	2.03 (0.81)	3.06 (1.16)	2.52 (0.97)	−1.68 (1.86)
$L22$	0.29 (0.15)	0.54 (0.17)	0.63 (0.19)	0.97 (0.09)	1.20 (0.22)	2.04 (0.12)	2.56 (0.15)	2.82 (0.12)	2.33 (0.06)
$L23$	−0.98 (0.11)	−1.19 (0.13)	−1.40 (0.15)	−2.04 (0.20)	−1.51 (0.20)	−1.31 (0.34)	−1.87 (0.48)	−1.38 (0.41)	1.91 (0.54)
$L33$	3.00 (0.10)	4.36 (0.11)	5.92 (0.13)	6.74 (0.16)	7.20 (0.15)	7.23 (0.23)	10.34 (0.35)	9.74 (0.30)	10.83 (1.04)
$S11$	−0.0002 (5)	−0.0003 (6)	−0.0004 (7)	−0.0004 (8)	−0.0006 (8)	−0.0005 (8)	−0.0003 (10)	−0.0004 (9)	0.0005 (8)
$S12$	−0.0005 (2)	−0.0004 (3)	−0.0004 (3)	−0.0005 (3)	−0.0004 (3)	−0.0016 (4)	−0.0016 (5)	−0.0013 (4)	0.0019 (4)
$S13$	0.0000 (1)	0.0001 (2)	0.0003 (2)	0.0002 (1)	0.0004 (2)	−0.0007 (2)	−0.0012 (3)	−0.0013 (3)	−0.0015 (5)
$S21$	−0.0001 (1)	−0.0002 (1)	−0.0004 (3)	−0.0005 (1)	−0.0005 (1)	−0.0004 (1)	−0.0007 (2)	−0.0004 (2)	0.0007 (2)
$S22$	−0.0002 (3)	−0.0002 (3)	−0.0002 (3)	−0.0005 (4)	−0.0002 (4)	−0.0002 (8)	−0.0005 (1)	−0.0003 (1)	0.0004 (1)
$S23$	0.0001 (2)	0.0001 (3)	0.0001 (2)	0.0001 (2)	0.0001 (2)	−0.0003 (1)	−0.0001 (1)	−0.0003 (1)	−0.0003 (2)
$S31$	0.0001 (1)	0.0002 (1)	0.0001 (2)	0.0000 (2)	−0.0001 (2)	−0.0011 (2)	−0.0011 (3)	−0.0015 (2)	−0.0017 (4)
$S32$	0.0007 (6)	0.0011 (1)	0.0015 (1)	0.0017 (8)	0.0018 (9)	0.0011 (5)	0.0017 (8)	0.0013 (6)	0.0014 (2)
$S33$	0.0004 (1)	0.0005 (1)	0.0006 (1)	0.0009 (1)	0.0008 (2)	0.0007 (1)	0.0008 (2)	0.0006 (2)	−0.0009 (4)
$\theta1$ (deg^2)	3.14	4.33	5.65	7.78	8.52	7.17	8.84	8.64	10.30
$\theta2$ ($^{\circ}$deg^2)	3.05	4.42	5.99	6.85	7.29	7.29	10.44	9.82	10.89
$\theta3$ (deg^2)	3.05	4.42	5.99	6.84	7.28	7.30	10.45	9.81	10.88
$\Gamma1$ (deg^2)	28	34.1	44.6	51.9	58.6	78.9	100.4	101.4	111.8
$\Gamma2$ (deg^2)	1.7	2.6	3.5	4.7	4.5	5.5	6.4	7.8	7.4
wR	0.038	0.035	0.032	0.03	0.028	0.022	0.026	0.021	0.020

Reliability index: $wR = [\sum w(U^{ij}_{obs} - U^{ij}_{calc})^2 / \sum w(U^{ij}_{obs})^2]^{1/2}$; $w = \sigma[\langle U^{ij}_{obs}\rangle]^{-2}$. Γi is given bySchomaker & Trueblood (1968).

axis is orthogonal to both I_1 and I_2 in the right-hand system of axes. In a first step, the *m*-CPA cation was considered as a rigid unit (rigid-body model; Schomaker & Trueblood, 1968). The large reliability wR factor [wR = 0.152 at 100 K (LTP) and 0.198 at 293 K (HTP)] shows that the *m*-CPA cation cannot be modelled as a rigid unit. Therefore, two librations ($\theta1$, $\theta2$) were added to describe the carboxylic group internal motion. ($\theta1$) describes the rotation of the carboxylic group around the C1—C2 bond, whereas $\theta2$ stands for a rotation around an axis perpendicular to C1—C2 in the phenyl ring plane. Another libration ($\theta3$) was added in the same way for the ammonium group. The rotation around C4—N1 cannot be modelled because the H atoms were refined isotropically (X-ray data). These hypotheses lead to excellent agreement; wR, decreased to 0.038 and 0.026 at 100 and 293 K respectively.

Table 2 summarizes the T, L and S parameters and the amplitudes of the refined internal vibrations with respect to the inertial coordinate system.

The amplitudes of translation and libration increase with increasing temperature as expected (Table 2). Indeed, the principal values of translation and libration amplitudes in the (HT) phase are about three times higher than those in the LTP (Figs. 8*a* and *b* **(AUTHOR - is Fig. 8 correct?)**.

The principal translation amplitudes (T^{11}, T^{22} and T^{33}) along the three perpendicular directions are almost equal in the LTP, the same trend is observed in the HTP and one can therefore note an isotropic behaviour (Table 2).

The two principal libration amplitudes L^{11} and L^{33}, which are nearly about the inertial axes I_1 and I_2 respectively, are distinctly higher than the third one, L^{22}, which is nearly about the inertial axis I_3. This has to be related to the rotation of the carboxylic group around the C1—C2 bond, as indicated by the important changes in the O1—C1—C2—C3, O1—C1—C2—C7, O2—C1—C2—C3 and O2—C1—C2—C7 torsion angles (Fig. 9*a* and *b*). Furthermore, L^{11} and L^{33} are respectively directed along the *a* and *b* crystallographic axes, which are the directions of the largest change of the thermal expansion/contraction. Indeed, the linear thermal expansion/contraction, along the *a* axis (α_a) decreases from 7.67 to 2.30 × 10^{-5} K^{-1} when the crystal undergoes the phase transition on heating, whereas (α_b) increases (three times) from 4.33 to 13 × 10^{-5} K^{-1} in absolute values (Bendeif *et al.*, 2005). The axial thermal expansion/contraction along the *c* axis (α_c) remains almost invariant in both LTP and HTP phases.

The rigid-body analysis indicates that the molecular motions originate more from the carboxylic group's internal motions than from the molecular translations and librations. The amplitudes of the molecular librations about the torsion axis (C5—C2) are compared with the mean-square amplitudes of the overall motions (libration + torsion) in Fig. 10. It follows that the amplitudes of the carboxylic group overall motions (Γ) are large at 100 K (28 deg^2) and grow enormously with temperature (111.8 deg^2 at 345 K), while the out-of-plane motions ($\Gamma2$) are more than one order of magnitude smaller

(Fig. 10*c*). They are thus crucial for understanding the thermal behaviour of the *m*-CPAMP crystal. It is to be noted once again that the transition is obvious from inspection of the molecular and internal motions *versus* temperature. The internal motions of the ammonium group may also contribute to the overall molecular motions, as shown before by the slope variation analysis, but being refined isotropically, the ammonium H atoms have not been included in the rigid-body analysis.

The rigid-body analysis of the phosphite group lead to wR = 0.19 and 0.07 at 100 (LTP) and 293 K (HTP), respectively. As observed for the *m*-CPA cation, the high values of the wR factor indicate that the ability of the TLS hypothesis to accurately describe the thermal displacements of the phosphite group is limited in relation; the different behaviours of the O3, O4 and O5 atoms were discussed previously. The inertial axes I'_1, I'_2 and I'_3 of the phosphite anion with respect to the crystallographic axes system are shown in Fig. 8(*b*). The elements of the rigid-body T, L and S tensors in the inertial axes frame for the phosphite anion are given in Table 3 of the supplementary material). The internal motions of the phosphite group are by no means negligible but cannot be estimated from the data available.

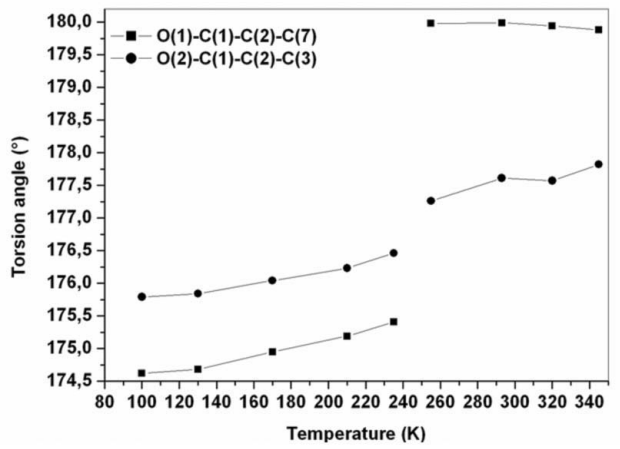

Figure 9
Temperature dependence of torsion angles (*a*) O1—C1—C2—C7 and O2—C1—C2—C3; (*b*) O1—C1—C2—C3 and O2—C1—C2—C7 torsion angles.

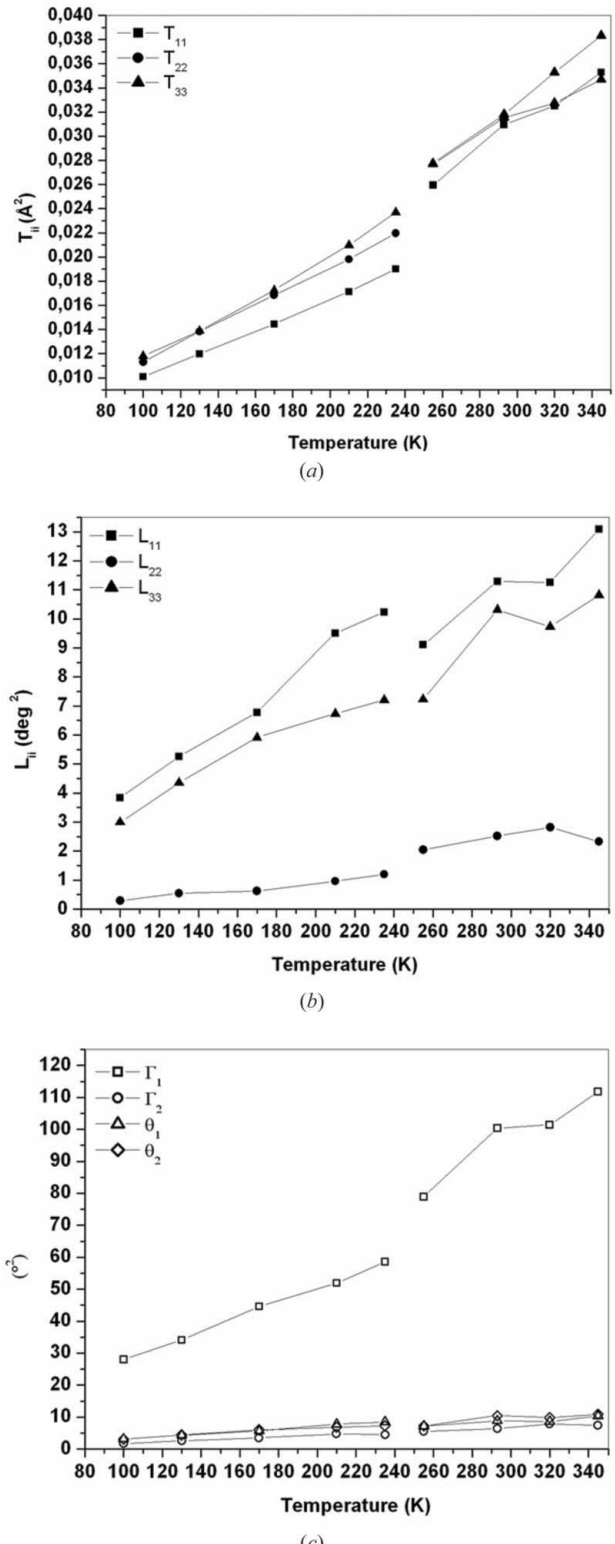

Figure 10
Temperature dependence of (*a*) the principal translation amplitudes, (*b*) the amplitudes of the principal molecular librations, and (*c*) the internal motions and the mean-square amplitudes of the overall mtions of the carboxylic group about the C5—C2 torsion axis.

4. Conclusion

In order to study the isosymmetric first-order phase transition of a *m*-CPAMP single-crystal X-ray structures have been determined over a wide temperature range (100–345 K) to better understand the phase transition mechanism and its origin.

The evolution of the bond lengths, hydrogen bonds and thermal displacement parameters are in line with the phase transition. They reveal a competition between the covalent character of the anion's and cation's covalent bonds and the (mostly hydrogen bonds) intermolecular interactions. The evolution of the isotropic Debye–Waller parameters exhibit different linear behaviour below and above the phase transition and the anisotropic displacement parameters analysis reveals that the magnitudes of the tensor components are stronger in the direction where the forces of cohesion are lower. On the other hand, most straight lines interpolate to negative values at 0 K for the high-temperature phase. This anomaly is a clear indicator of the presence of a phase transition.

The analysis of the slope variations for all non-H atoms provides detailed information about the non-rigid character of the molecule and reveals the close relationship between the vibrational behaviour of both N1 and O3 atoms, despite the strength of this weak hydrogen bond.

The results of the rigid-body analysis of the *m*-CPAMP crystal structures point out that the most important libration amplitudes in the crystalline *m*-CPAMP are directed along the directions of the largest change of the thermal expansion/contraction and are closely related to the important changes of the carboxylic group torsion angles.

This work was supported by the Université Henri Poincaré, Nancy Université and CNRS. We would like to thank the Service Commun de Diffraction X sur Monocristaux (Université Henri Poincaré, Nancy Université) for providing access to crystallographic experimental facilities. Authors are indebted to Professor Nourredine Benali-Cherif of Institut de Sciences Exactes, Technologie et Informatique Centre Universitaire de Khenchela, Algérie for many helpful discussions. We are also very grateful to A. Bouché and E. Wenger for their technical assistance. E. Bendeif is grateful to l'Agence Universitaire de la Francophonie (AUF) for a doctoral fellowship (Imputation coda: 1021FR412L).

References

Albers, J., Klopperpieper, A., Rother, H. J. & Haussuhl, S. (1988). *Ferroelectrics*, **81**, 27.
Baran, J., Czapla, Z., Drozd, M. K., Ilczyszyn, M. M., Marchewka, M. & Ratajczak, H. (1997). *J. Mol. Struct.* **403**, 17–37.
Baur, W. H. (1973). *Acta Cryst.* B**29**, 2726–2731.
Bendeif, E.-E., Dahaoui, S., François, M., Benali-Cherif, N. & Lecomte, C. (2005). *Acta Cryst.* B**61**, 700–709.
Boukhris, A., Lecomte, C., Wyncke, B., Brehat, F. & Thalal, A. (1994). *J. Phys. Condens. Matter*, **6**, 2475–2488.
Boukhris, A., Souhassou, M., Lecomte, C., Wyncke, B. & Thalal, A. (1998). *J. Phys. Condens. Matter*, **10**, 1621–1641.
Brittain, H. G. (2006). *J. Pharm. Sci.* **96**, 705–728.
Bürgi, H. B., Capelli, S. C. & Birkedal, H. (2000). *Acta Cryst.* A**56**, 425–435.
Burnett, M. N. & Johnson, C. K. (1996). *ORTEP*III. Report ORNL-6895. Oak Ridge National Laboratory, Tennessee, USA.
Cruickshank, D. W. J. (1956). *Acta Cryst.* **9**, 754–756.
Cyvin, S. J. (1968). *Molecular Vibrations and Mean Square Amplitudes.* Amsterdam: Elsevier.
Delarue, P., Lecomte, C., Jannin, M., Marnier, G. & Menaert, B. (1998). *Phys. Rev. B*, **58**, 5287–5295.
Delarue, P., Lecomte, C., Jannin, M., Marnier, G. & Menaert, B. (1999). *J. Phys. Condens. Matter*, **11**, 4123–4134.
DeTitta, G. T. (1985). *J. Appl. Cryst.* **18**, 75–79.
Dunitz, J. D., Maverick, E. F. & Trueblood, K. N. (1988). *Angew. Chem. Int. Ed. Eng.* **27**, 880–895.
Dunitz, J. D. & White, D. N. J. (1973). *Acta Cryst.* A**29**, 93–94.
Farrugia, L. J. (1999). *J. Appl. Cryst.* **32**, 837–838.
Herbstein, F. H. (2006). *Acta Cryst.* B**62**, 341–383.
Keeling, R. O. & Pepinsky, R. (1955). *Z. Kristallogr.* **106**, 236–265.
Kobayashi, J., Uesu, Y., Mizutani, I. & Enomoto, Y. (1970). *Phys. Status Solidi A*, **3**, 63–69.
Oxford Diffraction (2006). *CrysAlis CCD and CrysAlis RED.* Versions 1.171.31.7. Oxford Diffraction Ltd, Abingdon, Oxfordshire, England.
Rosenfield, R. E., Trueblood, K. N. & Dunitz, J. D. (1978). *Acta Cryst.* A**34**, 828–829.
Schomaker, V. & Trueblood, K. N. (1968). *Acta Cryst.* B**24**, 63–76.
Schomaker, V. & Trueblood, K. N. (1998). *Acta Cryst.* B**54**, 507–514.
Sheldrick, G. M. (2008). *Acta Cryst.* A**64**, 112–122.
Souhassou, M., Espinosa, E., Lecomte, C. & Blessing, R. H. (1995). *Acta Cryst.* B**51**, 661–668.
Trueblood, K. N. (1978). *Acta Cryst.* A**34**, 950–954.
Trueblood, K. N. (1990). *THMA*11. University of California, Los Angeles, USA.
Tuinstra, F. & Fraase Storm, G. M. (1978). *J. Appl. Cryst.* **11**, 257–259.